Antibody responses to Zika virus proteins in pregnant and non-pregnant macaques

Anna S. Heffron[1]†, **Emma L. Mohr[2]†**, David Baker[1], Amelia K. Haj[1], Connor R. Buechler[1], Adam Bailey[1], Dawn M. Dudley[1], Christina M. Newman[1], Mariel S. Mohns[1], Michelle Koenig[1], Meghan E. Breitbach[1], Mustafa Rasheed[1], Laurel M. Stewart[1], Jens Eickhoff[3], Richard S. Pinapati[4], Erica Beckman[4], Hanying Li[4], Jigar Patel[4], John C. Tan[4], David H. O'Connor[1]*

[1]Department of Pathology and Laboratory Medicine, University of Wisconsin-Madison, Madison, WI, United States of America

[2]Department of Pediatrics, School of Medicine and Public Health, University of Wisconsin-Madison, Madison, WI, United States of America

[3]Department of Biostatistics & Medical Informatics, University of Wisconsin-Madison

[4]Technology Innovation, Roche Sequencing Solutions, Madison, WI, United States of America

*Corresponding author

Email: dhoconno@wisc.edu (DHO)

†The first two authors contributed equally to this work.

Abstract

The specificity of the antibody response against Zika virus (ZIKV) is not well-characterized. This is due, in part, to the antigenic similarity between ZIKV and closely related dengue virus (DENV) serotypes. Since these and other similar viruses co-circulate, are spread by the same mosquito species, and can cause similar acute clinical syndromes, it is difficult to disentangle ZIKV-specific antibody responses from responses to closely-related arboviruses in humans. Here we use high-density peptide microarrays to profile anti-ZIKV antibody reactivity in pregnant and non-pregnant macaque monkeys with known exposure histories and compare these results to reactivity following DENV infection. We also compare cross-reactive binding of ZIKV-immune sera to the full proteomes of 28 arboviruses. We independently confirm a purported ZIKV-specific IgG antibody response targeting ZIKV nonstructural protein 2B (NS2B) that was recently reported in ZIKV-infected people and we show that antibody reactivity in pregnant animals can be detected as late as 127 days post-infection (dpi). However, we also show that these responses wane over time, sometimes rapidly, and in one case the response was elicited following DENV infection in a previously ZIKV-exposed animal. These results suggest epidemiologic studies assessing seroprevalence of ZIKV immunity using linear epitope-based strategies will remain challenging to interpret due to susceptibility to false positive results. However, the method used here demonstrates the potential for rapid profiling of proteome-wide antibody responses to a myriad of neglected diseases simultaneously and may be especially useful for distinguishing antibody reactivity among closely related pathogens.

Author summary

ZIKV has emerged as a vector-borne pathogen capable of causing serious illness in infected adults and congenital birth defects. The vulnerability of communities to future ZIKV outbreaks will depend, in part, on the prevalence and longevity of protective immunity, thought to be

mediated principally by antibodies. We currently lack diagnostic assays able to differentiate ZIKV-specific antibodies from antibodies produced following infection with closely related DENV, and we do not know how long anti-ZIKV responses are detectable. Here we profile antibodies recognizing linear epitopes throughout the entire ZIKV polyprotein, and we profile cross-reactivity with the proteomes of other co-endemic arboviruses. We show that while ZIKV-specific antibody binding can be detected, these responses are generally weak and ephemeral, and false positives may arise through DENV infection. This may complicate efforts to discern ZIKV infection and to determine ZIKV seroprevalence using linear epitope-based assays. The method used in this study, however, has promise as a tool for profiling antibody responses for a broad array of neglected tropical diseases and other pathogens and in distinguishing serology of closely-related viruses.

Introduction

Serologic assays designed to detect Zika virus (ZIKV) infection suffer from cross-reactivity with antibodies to closely related dengue virus (DENV), due to the high level of amino acid sequence identity (average ~55%) and structural similarity [1-4] between the two viruses. Humoral cross-reactivity with other similar arboviruses has been reported as well [1-2]. Serologic assays have been developed to detect past ZIKV infection, reporting sensitivity varying from 37% to 97% and specificity varying from 20% to 90% [5-8]. Most of these assays detect antibodies to the ZIKV envelope protein or nonstructural protein 1 (NS1) [7,9-11]. A recent publication by Mishra et al. employed a high-density peptide microarray to identify antibodies to linear ZIKV epitopes lacking cross-reactivity with other flaviviruses [12]. This group identified an IgG immunoreactive peptide sequence in the ZIKV nonstructural protein 2B (NS2B) which induced little antibody binding in serum from ZIKV-naive people and was bound in early convalescence in most cases

of symptomatic ZIKV infection [12]. This group did note seropositivity in a ZIKV-naive, DENV-immune individual and in one individual with no known flavivirus infection history.

Because ZIKV, DENV, and other arboviruses are similar in structure and acute clinical syndrome, are spread by the same mosquito vectors [13], and are co-endemic [14-15], it is difficult to identify people who have unequivocally been exposed to ZIKV only, adding uncertainty to efforts to profile ZIKV-specific antibody responses in humans. In contrast, macaques raised in indoor colonies can be infected specifically with ZIKV, DENV, or other pathogens. Macaque models of ZIKV infection provide a close approximation of human ZIKV infection in regards to natural history [16-19], tissue tropism [16-17,20-21], and transmission [17,22-25]. Importantly, macaques infected with ZIKV during pregnancy provide insight into the pathogenesis of congenital ZIKV infection [17-18,21-22,26-29]. Since the strain, dose, and timing of macaque model ZIKV infection is exactly known, the kinetics and specificity of humoral immune responses can be profiled in macaques with better resolution than is possible in cross-sectional human studies.

The peptide microarray technology we use in this study allows for one serum sample to be assayed against six million unique 16-residue peptides, or for 12 samples to each be assayed against 392,000 peptides, on a single chip (Roche Sequencing Solutions, Madison, WI). The technology has been used in proteome-wide epitope mapping [30], profiling of antibody responses in autoimmune disease [31], profiling venom toxin epitopes [32], determining functions of cellular enzymes [33], *de novo* binding sequence discovery [34], epitope validation following phage display screening [35], and screening for tick-borne disease seroprevalence [36]. We previously used this tool to examine antibody responses in simian pegivirus (SPgV) and simian immunodeficiency virus (SIV) infections [37]. As mentioned above, a recent

publication explored use of this technology in profiling human antibody responses against flaviviruses [12]. This linear peptide microarray technology has advantages over previous assays through its capacity to screen for reactivity to a large number of pathogens while simultaneously mapping reactive epitopes precisely, and it has the distinct advantage of allowing detection of unexpected epitopes due to its capacity to assay the entirety of a virus's proteome.

Here, we used high-density peptide microarrays to map macaque IgG epitopes in full-length ZIKV and DENV polyproteins and to compare cross-reactivity to 27 other arboviruses. Our study takes advantage of this technology's capacity to assess binding to linear epitopes throughout a virus' entire proteome to identify an epitope in ZIKV NS2B, a protein made intracellularly which embeds in the host cell's endoplasmic reticulum and thus would not be expected to induce strong antibody responses. We also demonstrate the potential of this technology, through its ability to survey binding throughout many whole viral proteomes simultaneously, to differentiate seroreactivity to an infecting virus from cross-reactivity against a great variety of other similar viruses. These unique aspects of this recently developed peptide microarray technology highlight its capacity to efficiently screen for and identify previously unknown epitopes in a large number of neglected disease-causing pathogens simultaneously and to distinguish infection histories of NTDs, potentially impacting the development of future diagnostics and vaccines.

Methods

Macaque study design

Animal demographics, inoculation strain, dose, and route, serum sample collection timelines, and array design used for each animal are described in Table 1. Gestational details and

116 outcomes for pregnant animals are described in Table 2. Additional details on the study

117 histories of the animals in this study can be found at https://go.wisc.edu/b726s1.

118

119 **Table 1.** Animal demographics.

Cohort	Animal	Public animal identifier*	Species	Sex	Flavivirus infection history	Inoculation strain	Inoculation dose and route	Time points of sample collection (days post infection, dpi)	Peptide array design
A	A1	cy0879	*Macaca fascicularis*	female	none	SIVmac239	7,000 TCID50, intrarectal	pre-infection, 125 dpi	Offset by 4, overlap of 12
	A2	cy0886	*Macaca fascicularis*	female	none	SIVmac239	7,000 TCID50, intrarectal	pre-infection, 126 dpi	Offset by 4, overlap of 12
B	B1	411359*	*Macaca mulatta*	female	none	Zika virus/H.sapiens-tc/FRA/2013/FrenchPolynesia-01_v1c1	10E4 PFU, subcutaneous	pre-infection, 28, 67 and 99 dpi	Offset by 1, overlap of 15
C	C1	295022*	*Macaca mulatta*	female	none	Zika virus/R.macaque-tc/UGA/1947/MR766-3329	10E4 PFU, subcutaneous	pre-infection, 28, 67 and 98 dpi	Offset by 1, overlap of 15
D	D1	448436*	*Macaca mulatta*	male	none	Zika virus/H.sapiens-tc/FRA/2013/FrenchPolynesia-01_v1c1	10E4 PFU, subcutaneous	pre-infection, 28 and 621 dpi	Offset by 1, overlap of 15
	D2	861138*	*Macaca mulatta*	female	none	Zika virus/H.sapiens-tc/FRA/2013/FrenchPolynesia-01_v1c1	10E4 PFU, subcutaneous	pre-infection, 28 and 582 dpi	Offset by 1, overlap of 15
F	F1	393422*	*Macaca mulatta*	male	Zika virus/H.sapiens-tc/FRA/2013/FrenchPolynesia-01_v1c1, 12 and 9.5 months prior	Dengue 2 New Guinea C	10E5 PFU, subcutaneous	pre-infection, 28 dpi	Offset by 4, overlap of 12
	F2	826226*	*Macaca mulatta*	male	Zika virus/H.sapiens-tc/FRA/2013/FrenchPolynesia-01_v1c1, 12 and 9.5 months prior	Dengue 2 New Guinea C	10E5 PFU, subcutaneous	pre-infection, 28 dpi	Offset by 4, overlap of 12
	F3	912116*	*Macaca mulatta*	male	Zika virus/H.sapiens-tc/FRA/2013/FrenchPolynesia-01_v1c1, 12 and 9.5 months prior	Dengue 2 New Guinea C	10E5 PFU, subcutaneous	pre-infection, 28 dpi	Offset by 4, overlap of 12
G	G1	660875*	*Macaca mulatta*	female	none	Zika virus/H.sapiens-tc/FRA/2013/FrenchPolynesia-01_v1c1	10E4 PFU, subcutaneous	pre-infection, 7, 21, 43, 78, 127 dpi	Offset by 1, overlap of 15

	G2	827577*	*Macaca mulatta*	female	none	Zika virus/H.sapiens-tc/FRA/2013/FrenchPolynesia-01_v1c1	10E4 PFU, subcutaneous	0, 7, 21, 35, 71, 113 days after primary infection	Offset by 4, overlap of 12
	H1	146523*	*Macaca mulatta*	female	none	Zika virus/H.sapiens-tc/PUR/2015/PRVABC59	10E4 PFU, subcutaneous	pre-infection, 7, 21, 70 dpi	Offset by 1, overlap of 15
	H2	858972*	*Macaca mulatta*	female	none	Zika virus/H.sapiens-tc/PUR/2015/PRVABC59	10E4 PFU, subcutaneous	pre-infection, 7, 21, 70 dpi	Offset by 1, overlap of 15
H	H3	419969*	*Macaca mulatta*	female	none	Zika virus/H.sapiens-tc/PUR/2015/PRVABC59	10E4 PFU, subcutaneous	pre-infection, 7, 21, 70 dpi	Offset by 1, overlap of 15
I	I1	776301*	*Macaca mulatta*	female	Dengue 3 Slenman/78, 9 months prior	Zika virus/H.sapiens-tc/PUR/2015/PRVABC59 bar code virus	10E4 PFU, subcutaneous	pre-infection, 8, 29, 57, 78 dpi	Offset by 4, overlap of 12

*Public animal identifiers are used in studies on the Zika Open Research Portal (https://zika.labkey.com/project/home/begin.view?).

Table 2. Gestational details.

Animal	Gestational days (gd) at inoculation	Pregnancy outcome
G1	36	delivery at 158 gd (122 dpi)
G2	38	delivery at 158 gd (120 dpi)
H1	46	fetectomy at 116 gd (70 dpi)
H2	47	fetectomy at 117 gd (70 dpi)
H3	43	fetectomy at 111 gd (68 dpi)
I1	35	delivery at 155 gd (120 dpi)

Ethics

All monkeys were cared for by the staff at the Wisconsin National Primate Research Center (WNPRC) in accordance with the regulations and guidelines outlined in the Animal Welfare Act and the Guide for the Care and Use of Laboratory Animals and the recommendations of the Weatherall report (https://royalsociety.org/topics-policy/publications/2006/weatherall-report/).

Per WNPRC standard operating procedures for animals assigned to protocols involving the experimental inoculation of an infectious pathogen, environmental enhancement included constant visual, auditory, and olfactory contact with conspecifics, the provision of feeding devices which inspire foraging behavior, the provision and rotation of novel manipulanda (e.g., Kong toys, nylabones, etc.), and enclosure furniture (i.e., perches, shelves). Per Animal Welfare Regulations (Title 9, Chapter 1, Subchapter A, Parts 1–4, Section 3.80 Primary enclosures) the animals were housed in a nonhuman primate Group 3 enclosure with at least 4.3 square feet of floor space and at least 30 inches of height. This study was approved by the University of Wisconsin-Madison Graduate School Institutional Animal Care and Use Committee (animal protocol numbers G005401 and G005443).

Virus stocks

SIVmac239 (GenBank accession: M33262) stock was prepared by the WNPRC Virology Services Unit. Vero cells were transfected with the SIVmac239 plasmid. Infectious supernatant was then transferred onto rhesus PBMC. The stock was not passaged before collecting and freezing. ZIKV strain H/PF/2013 (GenBank accession: KJ776791) was obtained from Xavier de Lamballerie (European Virus Archive, Marseille, France) and passage history is described in Dudley et al. [16]. ZIKV strain MR766, ZIKV strain PRVABC59, and DENV-2 strain New Guinea C were generously provided by Brandy Russell (CDC, Ft. Collins, CO). ZIKV strain MR766 passage history has been described in Aliota et al. [38]. A molecularly-barcoded version of ZIKV strain PRVABC59 (Zika virus/H.sapiens-tc/PUR/2015/PRVABC59; GenBank accession: KU501215) was constructed as described in Aliota et al. [39]. DENV-2 strain New Guinea C (GenBank accession: FJ390389), originally isolated from a human in New Guinea, underwent 17 rounds of amplification on cells and/or suckling mice followed by a single round of amplification on C6/36 cells; virus stocks were prepared by inoculation onto a confluent

154 monolayer of C6/36 mosquito cells. DENV-3 strain Sleman/78 was obtained from the NIH; virus
155 stocks were prepared by a single passage on C6/36 cells.

156 **Multiple sequence alignment**

157 Full-length ZIKV and DENV polyprotein sequences were extracted from the National Center for
158 Biotechnology Information (NCBI) database into Geneious Pro 9.1.8 (Biomatters, Ltd.,
159 Auckland, New Zealand). These sequences included the ZIKV and DENV polyprotein
160 sequences described above (see “Virus stocks”), as well as DENV-1 strain VR-1254 (GenBank
161 accession: EU848545) and DENV-4 strain VID-V2055 (GenBank accession: KF955510). These
162 amino acid sequences were aligned using the Geneious alignment algorithm as implemented in
163 Geneious Pro 9.1.8 using default parameters (global alignment with free end gaps, cost matrix:
164 Blosum62).

165 **Peptide array design and synthesis**

166 Viral protein sequences were selected and submitted to Roche Sequencing Solutions (Madison,
167 WI) for development into a peptide microarray as part of an early access program. Sequences
168 included three ZIKV polyproteins (an Asian strain, ZIKV-FP, GenBank accession: KJ776791.2;
169 an African strain, ZIKV-MR766, GenBank accession: KU720415.1; and an American strain,
170 ZIKV-PR, GenBank accession: KU501215.1), four DENV polyproteins (DENV-1, GenBank
171 accession: EU848545.1; DENV-2, GenBank accession: KM204118.1; DENV-3, GenBank
172 accession: M93130.1; and DENV-4, GenBank accession: KF955510.1), and one SIVmac239
173 env protein (GenBank accession: AAA47637.1), which were used for most analyses in this
174 study. Sequences used for cumulative distribution function (CDF) plots (see Figure 3) and
175 analysis include sequences for mosquito-borne viruses found in Africa and known to infect
176 humans [40], as well as one Japanese encephalitis virus strain (GenBank accession:
177 KX945367.1). Accession numbers used to represent each viral protein are listed in the

supplemental material (Table S7). Proteins were tiled as non-redundant 16 amino acid peptides, overlapping by 12 or 15 amino acids. The array designs are publicly available at https://go.wisc.edu/b726s1.

The peptide sequences were synthesized *in situ* with a Roche Sequencing Solutions Maskless Array Synthesizer (MAS) by light-directed solid-phase peptide synthesis using an amino-functionalized support (Geiner Bio-One) coupled with a 6-aminohexanoic acid linker and amino acid derivatives carrying a photosensitive 2-(2-nitrophenyl) propyloxycarbonyl (NPPOC) protection group (Orgentis Chemicals). Unique peptides were synthesized in random positions on the array to minimize impact of positional bias. Each array is comprised of twelve subarrays, where each subarray can process one sample and each subarray contains up to 392,318 unique peptide sequences.

Peptide array sample binding

Macaque serum samples were diluted 1:100 in binding buffer (0.01M Tris-Cl, pH 7.4, 1% alkali-soluble casein, 0.05% Tween-20). Diluted sample aliquots and binding buffer-only negative controls were bound to arrays overnight for 16-20 h at 4°C. After binding, the arrays were washed 3x in wash buffer (1x TBS, 0.05% Tween-20), 10 min per wash. Primary sample binding was detected via 8F1-biotin mouse anti-primate IgG (NIH Nonhuman Primate Reagent Resource) secondary antibody. The secondary antibody was diluted 1:10,000 (final concentration 0.1 ng/µl) in secondary binding buffer (1x TBS, 1% alkali-soluble casein, 0.05% Tween-20) and incubated with arrays for 3 h at room temperature, then washed 3x in wash buffer (10 min per wash) and 30 sec in reagent-grade water. The secondary antibody was labeled with Cy5-Streptavidin (GE Healthcare; 5 ng/µl in 0.5x TBS, 1% alkali-soluble casein, 0.05% Tween-20) for 1 h at room temperature, then the array was washed 2x for 1 min in 1x

TBS, and washed once for 30 sec in reagent-grade water. Fluorescent signal of the secondary antibody was detected by scanning at 635 nm at 2 µm resolution and 25% gain, using an MS200 microarray scanner (Roche NimbleGen).

Peptide array data processing

The datafiles and analysis code for figures are available from https://go.wisc.edu/b726s1. All figures use the log base 2 of the raw fluorescence signal intensity values. For each sample, each unique peptide was assayed and processed once; then results from peptides redundant to multiple proteomes (i.e. were present in more than one strain represented) were restored to each protein.

For cumulative distribution function (CDF) plots, fluorescence signal intensities were log base 2 transformed and background reactivity in the blank (binding buffer only) control sample was subtracted for each peptide. The fold change from 0 dpi was calculated by subtracting reactivity at 0 dpi from reactivity at 28 dpi. To reduce instrument-related variance, the data was then filtered by taking the minimum intensity of two consecutive peptides with 1 amino acid offset, thereby reducing peptide outliers by ensuring measured reactivity occurs in multiple consecutive peptides.

Validation of peptide array findings

To confirm the validity of our findings from this recently-developed peptide microarray platform, we assessed its performance against the humoral response produced by infection with simian immunodeficiency virus (SIV), which has been well-characterized by conventional methods such as enzyme-linked immunosorbent assays (ELISAs), enzyme-linked immunosorbent spot assays (ELISPOTs), epitope-prediction methods, or other protein arrays. We synthesized linear 16-mer

peptides, overlapping by 12 amino acids, representing the SIVmac239 envelope protein (env) and analyzed serum from two Mauritian cynomolgus macaques for SIV-specific IgG reactivity before and approximately 125 days after SIVmac239 infection (Table 1). (We have previously plotted data procured from peptide array assays of these samples [37] while investigating the antibody response to SIV in the context of simian pegivirus infection; here we show the same data using the updated, improved data processing pipeline described above). Post-infection samples showed fluorescence intensity as high as 1,000 times the intensity in pre-infection samples (Supplemental figure S1). Regions of higher-fold increases in fluorescence intensity corresponded to previously defined variable domains of env which are known antibody targets, the variable loop regions, as well as others corresponding to known epitopes [41,42]. Taken together, these results validate epitope definition on the peptide microarray platform and show this platform to be capable of high-resolution virus-specific IgG epitope identification using the analytic methods utilized here.

Results

Identification of linear B cell epitopes in the ZIKV polyprotein

We sought to determine antibody binding, or reactivity, to the ZIKV polyprotein following ZIKV infection. We tiled 16-residue (16-mer) peptides overlapping by 15 amino acids representing different ZIKV polyproteins and evaluated the antibody binding of serum samples from animals with recent ZIKV-FP (animals B1, D1, and D2) or ZIKV-MR766 (animal C1) infections (Table 1). Animals in both groups had demonstrated neutralizing antibody responses at 28 dpi, measured by 90% plaque reduction neutralization tests ($PRNT_{90}$) as described previously [16,38,23]. Peptides were defined as reactive if the signal intensity was greater after infection with a cognate strain (e.g., increased signal intensity against ZIKV peptides in an animal infected with

ZIKV) than it was before infection. Peptides were defined as cross-reactive if the signal intensity was greater after infection with a noncognate strain (e.g., increased signal intensity against ZIKV peptides in an animal infected with DENV). Statistical significance of the change in signal intensity versus no change was calculated using a two-tailed log-ratio t-test. True epitopes were expected to induce antibody binding to multiple peptides with overlapping sequences; thus regions were only considered epitopes when there was a statistically significant increase in intensity in a post-infection sample relative to intensity in a pre-infection sample in three or more consecutive peptides.

Reactivity was most commonly observed in three regions of the flavivirus polyprotein: envelope protein, NS2B, and nonstructural protein 3 (NS3); therefore, most of the analysis in this paper is limited to these regions. Antibody binding to peptides from the envelope protein was seen in all four animals at 28 dpi; antibody binding in the NS3 region was seen in three out of four animals (Figure 1; reactivity throughout the entire ZIKV polyprotein can be seen in supplemental figure S2). The four animals exhibited similar responses against an Asian ZIKV strain, ZIKV-FP (Figure 1), as against an African strain and an American strain (ZIKV-MR766 and ZIKV-PR respectively, supplemental figure S3).

Figure 1. Reactivity of ZIKV-convalescent animals against the ZIKV-FP polyprotein. Serum from rhesus macaques infected with ZIKV-FP (animals B1, D1, and D2) and with ZIKV-MR766 (animal C1) was assayed for IgG recognition of the ZIKV-FP polyprotein. Reactivity prior to infection and at 28 dpi is shown. The $NS2B_{1427\text{-}1451}$RD25 epitope is highlighted in grey.

All four animals exhibited antibody binding to the ZIKV NS2B epitope similar to that documented in humans [12]. Though other reactive epitopes were identified in other proteins in multiple

animals, this epitope was the only epitope in our study for which all ZIKV-infected animals showed reactivity. All ten ZIKV-infected animals in this study were used to determine statistical significance of this epitope in order to avoid making statistical inferences using very small sample sizes [43]. Area under the curve (AUC) values and corresponding receiver operating characteristic (ROC) curves were calculated (supplemental figure S4) to identify ten peptides at positions 1427-1436 in the polyprotein (for a total of 25 amino acids, sequence RAGDITWEKDAEVTGNSPRLDVALD) as the best-performing epitope for which a statistically significant change from 0 dpi was observed, hereafter referred to as $NS2B_{1427\text{-}1451}$RD25 (AUC of 0.9375, 95% confidence interval of 0.89065 to 0.9375). Using the mean signal intensity across the ten peptides, the change of signal intensity from 0 dpi to 21-28 dpi was statistically significant versus no change by a two-tailed log-ratio t-test (p-value = 0.000501 < 0.05, df = 9). This epitope is slightly longer than that found by Mishra et al. (nine 12-mer peptides, for a total of 20 amino acids, sequence DITWEKDAEVTGNSPRLDVA) [12].

Cross-reactivity of ZIKV-convalescent serum with DENV polyproteins and with arbovirus proteomes

DENV polyproteins share an average of 55% sequence identity with ZIKV polyproteins [1,2], and the region of DENV NS2B corresponding to the immunoreactive ZIKV $NS2B_{1427\text{-}1451}$RD25 epitope shares an average of 41% identity (Figure 2 A). To examine cross-reactivity, we analyzed the antibody binding of samples from the ZIKV-convalescent animals against DENV polyproteins represented on the array (Figure 2 B-E). Cross-reactivity was apparent, with antibodies from the ZIKV-convalescent/DENV-naive animals recognizing regions of DENV polyproteins. All four animals showed some cross-reactivity against the DENV envelope protein and DENV NS3. Animals exhibited comparable cross-reactivities to all four DENV serotypes, with the highest single instance of cross-reactivity observed against a DENV-3 epitope in the

297 NS3 region. No significant cross-reactivity against the DENV NS2B protein was observed for
298 these or any ZIKV-infected animals in this study (p-value = 0.548, df = 9).
299
300 **Figure 2**. Cross-reactivity of ZIKV-convalescent animals against polyproteins of the four DENV
301 serotypes. DENV serotypes share an average of 41% sequence similarity with the aligned ZIKV
302 NS2B epitope (A). Serum from rhesus macaques infected with ZIKV-FP (animals B1, D1, and
303 D2) or ZIKV-MR766 (C1) was assayed for cross-reactivity against polyproteins of DENV
304 serotypes 1-4 (B-E, respectively). The segment of DENV NS2B which aligns with the ZIKV
305 $NS2B_{1427\text{-}1451}$RD25 epitope is highlighted in grey.
306
307 Given this array's capacity to screen for antibody binding to peptides representing many
308 different virus proteomes at once, we also assessed cross-reactivity against the 27 other
309 arboviruses (for a total of 28 arboviruses) represented. We plotted the fold change in reactivity
310 from 0 to 28 dpi for each peptide in each virus's proteome using cumulative distribution function
311 (CDF) plots (Figure 3). CDF plots were used to determine whether the sum of reactivity across a
312 viral proteome could distinguish reactivity to the infecting pathogen (in this case, ZIKV) from
313 cross-reactivity to a variety of other similar or dissimilar pathogens (in this case, 27 other
314 arboviruses). Cross-reactivity in peptides in other arboviruses was observed, but it was rare
315 compared with the reactivity seen in the ZIKV peptides. The greatest degree of cross-reactivity
316 occurred among flaviviruses, in particular Ntaya virus, Spondweni virus, Bagaza virus, and
317 DENV-3 (Figure 3 C). Pooled t-tests showed significant differences between reactivity against
318 ZIKV strains and other viruses for each of the four animals (Table 3). In animal B1, reactivity
319 against ZIKV was significantly different from cross-reactivity against all other arboviruses (p-
320 values ranging from <0.0001 to 0.0006). Animal C1's reactivity against ZIKV was significantly
321 different (p-values <0.05) for all viruses assayed except Babanki virus, Banzi virus, DENV-4,

Uganda S virus, and yellow fever virus. D1 showed reactivity against ZIKV that was significantly different from reactivity against all other viruses except Spondweni virus. D2 showed more significant cross-reactivity with other arboviruses; in D2, ZIKV reactivity differed significantly from reactivity to all other viruses except Bwamba virus, Chikungunya virus, DENV-1, Middelburg virus, Ndumu virus, Rift Valley fever virus, Spondweni virus, and Uganda S virus. Of note, D2 did also exhibit the smallest increase in fold change from 0 to 28 dpi in reactivity against ZIKV; this higher likelihood of cross-reactivity may be attributable to the minimal overall amount of reactivity present. Reactivity for the two ZIKV strains compared, one African strain (ZIKV-MR766, GenBank accession: NC_012532.1) and one Asian/American strain (GenBank accession: NC_035889.1) was not significantly different for any animal (p-values ranging from 0.62 to 0.88).

Figure 3. Cross-reactivity of sera from ZIKV-convalescent animals against the complete polyproteins or proteomes of 27 arboviruses represented on the array. Cumulative distribution function (CDF) plots of fold change from 0 dpi to 28 dpi by of animals' reactivity and cross-reactivity to different viral proteomes are shown; data for animals infected with ZIKV-FP (B1, D1, and D2) and ZIKV-MR766 (C1) are shown. Reactivity to two ZIKV strains, one African and one Asian/American, is compared against all viruses on the array of order Bunyavirales (A), of family Togaviridae (B), of family Flaviviridae (C), and with the averages of reactivity of all viruses in Bunyavirales, of all viruses in Togaviridae, and of all viruses in Flaviviridae (D). The region of interest is shown large in the figure, while the full CDF plot is shown as an inset. ZIKV strains demonstrate significantly increased fold change in reactivity compared to the majority of other viruses represented on the array (see Table 3).

Table 3. Significance of difference from ZIKV of summed reactivity.

	p-value for t-test against Asian/American ZIKV strain			
Arbovirus species	**B1**	**C1**	**D1**	**D2**
Babanki	<0.0001	0.0924*	0.0188	0.0004
Bagaza	<0.0001	0.0010	0.0001	<0.0001
Banzi	<0.0001	0.0609*	0.0060	0.0062
Bunyamwera	<0.0001	0.0094	0.0001	0.0202
Bwamba	<0.0001	0.0019	0.0030	0.2367*
Chikungunya	<0.0001	0.0452	0.0002	0.0562*
Dengue 1	<0.0001	0.0010	0.0015	0.2522*
Dengue 2	<0.0001	0.0006	0.0053	0.0074
Dengue 3	0.0001	0.0067	0.0017	<0.0001
Dengue 4	<0.0001	0.1880*	<0.0001	0.0038
Japanese encephalitis	0.0002	0.0349	0.0045	0.0447
Middelburg	<0.0001	0.0081	0.0006	0.2074*
Ndumu	<0.0001	0.0008	<0.0001	0.1681*
Ngari	<0.0001	0.0110	0.0015	0.0997*
Ntaya	0.0002	0.0002	<0.0001	0.0476
Nyando	<0.0001	0.0027	<0.0001	0.0001
Rift Valley fever	<0.0001	0.0085	0.0001	0.1868*
Semliki Forest	<0.0001	0.0118	<0.0001	0.0053
Sindbis	<0.0001	0.0417	0.0010	<0.0001
Spondweni	0.0006	0.0015	0.5734*	0.2896*
Uganda S	<0.0001	0.0608*	<0.0001	0.2134*
Usutu	<0.0001	0.0129	0.0084	0.0053
Wesselsbron	<0.0001	0.0032	0.0005	0.0002
West Nile lineage 1	<0.0001	0.0007	0.0035	<0.0001
West Nile lineage 2	<0.0001	0.0009	0.0052	0.0016
Witwatersrand	<0.0001	0.0083	0.0034	0.0289
Yellow fever	<0.0001	0.5379*	0.0003	0.0002
Zika, African	0.7952*	0.6184*	0.8688*	0.7304*

*Non-significant values (p-value > 0.05).

Anti-ZIKV antibody response during pregnancy

Given the importance of determining an accurate ZIKV infection history in pregnancy, we sought to characterize the gestational anti-ZIKV antibody response. We used the peptide microarray to evaluate serum samples from six pregnant animals. Animals were inoculated with ZIKV at 35-47 days post-conception (gestational date, gd) (Table 2). Two animals (G1 and G2) had no history of flavivirus exposure and were inoculated with ZIKV-FP at 36-38 gd. Three more flavivirus-naive animals (H1, H2, and H3) were infected with ZIKV-PR at 45-47 gd. One animal (I1) had a history of exposure to DENV-3 nine months prior to inoculation with a barcoded clone of ZIKV-PR at 35 gd [39]. Serum samples collected approximately one week post-infection and at two to six week intervals thereafter were analyzed against ZIKV polyproteins represented on the peptide array (Figure 4). All six pregnant animals exhibited anti-NS2B$_{1427\text{-}1451}$RD25 reactivity by the early convalescent phase (21-29 dpi), though time of initial appearance and duration of the response varied between animals.

Figure 4. IgG reactivity against ZIKV NS2B$_{1427\text{-}1451}$RD25 during pregnancy. Serum samples taken throughout the course of six animals' pregnancies were evaluated against the ZIKV-FP polyprotein represented on peptide microarrays. Two animals (G1 and G2) were infected with ZIKV-FP at 36-38 gd. Three animals (H1, H2, H3) were infected with ZIKV-PR at 45-47 gd. One animal (I1) had been infected with DENV-3 nine months prior and was infected with a barcoded clone of ZIKV-PR at 35 gd. The NS2B$_{1427\text{-}1451}$RD25 epitope is highlighted in grey. Reactivity against the ZIKV-FP envelope and NS3 proteins can be found in supplemental figure S5.

All pregnant animals showed a similar pattern of anti-ZIKV reactivity, with some differences in time to peak reactivity and duration of detectable reactivity. In G1, elevated baseline intensity in the ZIKV NS2B$_{1427\text{-}1451}$RD25 region was present prior to inoculation with ZIKV-FP. Reactivity peaked in the acute phase (7 dpi) and subsequently decreased but remained above pre-

374 infection levels through 127 dpi, after G1 had given birth. In G2, reactivity was not appreciable
375 until the early convalescent phase (21 dpi) and peaked at 35 dpi, remaining elevated relative to
376 pre-infection levels through the latest time point analyzed (113 dpi). Animals H1 and H3 showed
377 elevated pre-infection intensity against NS2B$_{1427\text{-}1451}$RD25. All three animals in cohort H showed
378 reactivity by 21 dpi. H1 and H2 continued to exhibit increased reactivity through the latest time
379 point measured (70 dpi), while H3 had peak reactivity at 21 dpi and decreased after. I1, an
380 animal nine months post-DENV-3 infection, showed a pattern of reactivity similar to that in other
381 animals, with anti-NS2B$_{1427\text{-}1451}$RD25 IgG reactivity first appearing at 8 dpi and peaking at 29 dpi
382 at a level 3.6 times pre-infection reactivity (Figure 4). Reactivity remained close to peak
383 reactivity through 78 dpi.
384
385 All pregnant animals' cross-reactivity against DENV polyproteins mirrored that seen in non-
386 pregnant animals (supplemental figure S6).

387 **Differentiating DENV serology in ZIKV-immune animals**

388 Previous assays have struggled to distinguish DENV serologic responses from ZIKV serologic
389 responses [5-8]. We investigated whether the peptide microarray technology, and specifically
390 reactivity patterns using the ZIKV NS2B$_{1427\text{-}1451}$RD25 epitope, could distinguish DENV from ZIKV
391 infections. Three animals (cohort F) had been challenged twice with ZIKV-FP 12 months prior
392 and 9.5 months prior [16]; we collected serum from these animals, infected them with DENV-2,
393 and collected serum 28 days after. These samples were analyzed against 16-mer peptides, with
394 amino acid overlap of 12, representing DENV-2 and ZIKV-FP (Figure 5).
395
396 **Figure 5.** Antibody reactivity to DENV and ZIKV polyproteins of animals with recent DENV
397 infection. Three macaques (F1, F2, and F3), with history of challenge and rechallenge with

ZIKV-FP 12 and 9.5 months prior, were infected with DENV-2 and serum samples taken before DENV infection and at 28 dpi were assessed. Reactivity of these animals against peptides representing the envelope, NS2B, and NS3 proteins of DENV-2 (A) and ZIKV-FP (B) is shown. The ZIKV $NS2B_{1427\text{-}1451}$RD25 epitope (in B) is highlighted in grey.

These animals showed reactivity against all four DENV polyproteins in regions representing the DENV envelope protein, DENV NS3, and others (Figure 5A) and cross-reactivity against corresponding regions of the ZIKV polyprotein (Figure 5B). One animal (F3) out of the three showed significant reactivity to the $NS2B_{1427\text{-}1451}$RD25 epitope, though this reactivity was slightly outside the area of typical $NS2B_{1427\text{-}1451}$RD25 reactivity (peptides 1421-1444 rather than 1427-1451). Another (F1) showed elevated pre-DENV infection intensity in $NS2B_{1427\text{-}1451}$RD25 that did not change following DENV infection, possibly as a result of the animal's prior ZIKV exposure. Animal F2 showed no detectable $NS2B_{1427\text{-}1451}$RD25 reactivity before or after exposure.

Discussion

We describe the antibody binding of the anti-ZIKV IgG response in non-pregnant and pregnant rhesus macaques and compare this to the anti-DENV response. Using a recently developed high-density peptide microarray we show that macaques infected with ZIKV produce IgG antibodies which bind throughout the ZIKV polyprotein, including conserved antibody binding to an epitope in ZIKV NS2B, $NS2B_{1427\text{-}1451}$RD25, which is apparent regardless of the ZIKV strain used for infection. We establish that cross-reactivity exists between anti-ZIKV and anti-DENV antibodies for the ZIKV and DENV polyproteins, and we show this technology can be used to differentiate anti-ZIKV reactivity from cross-reactivity to many other arboviruses. Additionally, we show the anti-$NS2B_{1427\text{-}1451}$RD25 IgG response is susceptible to false positives in the context of DENV infection and may be susceptible to false-positives in flavivirus-immune individuals. Thus,

while this epitope may be broadly useful for serosurveillance, it should be used with caution in the diagnosis of individual infections.

As has been seen in previous assays [2,12,44-46], we observed antibody cross-reactivity between ZIKV- and DENV-immune sera, though reactivity to the ZIKV NS2B$_{1427\text{-}1451}$RD25 epitope was observed in all cases of recent ZIKV infection (10 out of 10 ZIKV-infected animals), and in only one out of three cases of recent DENV infection in animals with history of ZIKV exposure. Reactivity to the NS2B epitope was conserved whether the infecting strain was African, Asian, or American in origin. All ZIKV-infected animals produced anti-ZIKV IgG against the NS2B$_{1427\text{-}1451}$RD25 epitope, though reactivity was sometimes small in magnitude (as in animal D2) or was measurable for only a short duration (as in animal H3). The lack of uniformity of the anti-ZIKV IgG response is especially relevant since all ZIKV-exposed animals could be followed, in contrast to studies in humans where there may be a selection bias for individuals with symptomatic ZIKV, which is thought to account for only approximately half of ZIKV infections [12,47]. Though anti-NS2B$_{1427\text{-}1451}$RD25 reactivity was consistently detectable in early convalescence, it decayed in all but one case, that of a pregnant animal with previous DENV exposure, during the time period assessed. These findings corroborate findings in humans, in which symptomatic ZIKV infection was strongly associated with detectable anti-NS2B antibodies in the early convalescent phase (96%), but was less likely six months post-infection (44%) [12]. These results demonstrate the need for further investigation into the longevity and kinetics of the anti-ZIKV humoral response. Given that no other purported ZIKV-specific epitopes have been identified to date, these results also call into question how useful current serological methods may be in differentiating past ZIKV exposure from exposure to other flaviviruses. Additionally, one animal (F3) with a history of previous ZIKV infections showed reactivity against the ZIKV NS2B$_{1427\text{-}1451}$RD25 epitope following experimental DENV infection, indicating that a history of ZIKV infection or a recent DENV infection has potential to confound results using this

448 epitope. Thus, while this epitope appears to be more ZIKV-specific than most, its utility in
449 guiding development of diagnostics will likely be limited.
450
451 The ability of the peptide array to differentiate seroreactivity against ZIKV from cross-reactivity
452 to other viruses and to show cross-reactivity to 27 other mosquito-borne arboviruses suggests
453 this technology, with additional optimization, could be useful for determining the etiology of fever
454 of unknown origin and other non-specific symptoms in areas where mosquito-borne diseases
455 are common. All ZIKV-infected animals showed the greatest fold change in reactivity against
456 ZIKV proteomes. Though these differences in fold change did not always reach significance for
457 all strains in all animals, the tendency to show the greatest reactivity in ZIKV strains, even in
458 comparisons against very closely-related flaviviruses, for ZIKV-infected animals demonstrates
459 the potential of this technology in guiding diagnostic development in the future.
460
461 This assay detected anti-NS2B$_{1427\text{-}1451}$RD25 reactivity in all pregnant macaques exposed to
462 ZIKV. Production of IgG antibodies has relevance to both mother and fetus, since maternal IgG
463 crosses the placenta and transport of IgG across the placental barrier increases throughout the
464 course of pregnancy [48]. It can be presumed the anti-ZIKV IgG produced by these animals also
465 reached their fetuses, but whether these anti- NS2B$_{1427\text{-}1451}$RD25 antibodies provide protection,
466 contribute to the pathogenesis of ZIKV disease and ZIKV congenital effects, or are irrelevant in
467 ZIKV pathology is currently unknown. Though we did not note any variation in outcomes with
468 differences in antibody responses, it is possible deviations in antibody responses during
469 pregnancy could help explain differences in outcomes following gestational ZIKV infection.
470 Several pregnant animals also showed elevated pre-infection intensity at the NS2B$_{1427\text{-}1451}$RD25
471 epitope. This phenomenon may be due to innate immunodominance of the NS2B$_{1427\text{-}1451}$RD25
472 epitope, or it may be due to molecular mimicry, though we have not found this epitope present

473 in any other pathogen. These findings merit further and more thorough investigation than this
474 current study can provide.
475
476 The peptide array technology used in this study has several limitations. The assay's utility could
477 be increased by the addition of quantitative capacities. We currently use a 1:100 antibody
478 dilution since we have found this to produce an optimal signal:noise ratio, but it is possible serial
479 dilutions could allow for measurement of quantitative results. Greater confidence in this assay's
480 results could be derived from assessing its ability to identify the binding of well-characterized
481 monoclonal antibodies. Once validated in this way, the array could then be used to determine
482 the specificity of new monoclonal antibodies as they are discovered. Additionally, our study
483 defined a positive response as an increase from an animal's pre-infection intensity; human
484 patients usually cannot give pre-infection samples and must rely upon controls determined from
485 humans having no known history of exposure to certain pathogens. The development of such a
486 control would raise the specificity of the assay at the expense of sensitivity, and thus would risk
487 missing some true positive results when definitive pre-infection samples from the same
488 individual are not available.
489
490 The peptide array approach is also limited due to its reliance on continuous linear epitopes.
491 Many documented ZIKV epitopes are conformational discontinuous epitopes [49-55]. Other
492 epitope discovery methods will likely remain superior in defining discontinuous epitopes, but this
493 technology is useful in identifying immunoreactive regions not previously considered as potential
494 epitopes. Past work from our laboratory, including results from some of the animals whose sera
495 was analyzed here, has shown anti-ZIKV neutralizing antibody titers measured by $PRNT_{90}$ do
496 not drop off but remain elevated as late as 64 dpi [16]. The discordance between levels of anti-
497 $NS2B_{1427\text{-}1451}$RD25 IgG and neutralizing antibody titers may indicate the anti-$NS2B_{1427\text{-}1451}$RD25

antibodies do not play a role in protection against future infections, which may explain the drop-off in their production observed in macaques and in humans.

In the future, this technology could be expanded for use in profiling antibody responses to many other pathogens. This tool was able to detect known and previously unknown epitopes throughout the ZIKV proteome, including epitopes in unexpected regions such as NS2B. This approach could be applied to other NTDs to advance diagnostic and vaccine development. The array used in this study simultaneously evaluates antibody responses against the entire proteomes of every mosquito-borne virus known to infect humans in Africa. Building off what we have learned through this and other peptide array analyses, we intend to use this array to survey antibody reactivity in African populations, through which we may identify previously unknown epitopes for some of the rare pathogens represented on the array. Additionally, we plan to use this assay to evaluate and compare both IgM and IgG responses in these analyses, which may help elucidate the kinetics of the immediate and long-term antibody response to pathogens.

In summary, this work in macaques demonstrates the capacity of a recently developed peptide microarray to profile the binding of distinct anti-ZIKV and anti-DENV IgG antibody responses in experimental infections. Our work shows the anti-NS2B$_{1427\text{-}1451}$RD25 IgG response is characterized by relatively rapid decay and is susceptible to confounding, mirroring results seen in humans. The peptide microarray technology used shows particular promise in evaluating full-proteome antibody binding for a large number of pathogens efficiently and may be especially useful for neglected tropical diseases for which diagnostics are rudimentary or non-existent.

Acknowledgments

We would like to thank Adam Ericsen for helpful discussions.

Grant support: National Institutes of Health grants R01AI116382 and R24OD017850 (ASH, AKH, CRB, AB, DMD, CMN, MK, MEB, MR, LMS, DHO) and the Pediatric Infectious Diseases Society Fellowship Award funded by Stanley A. Plotkin and Sanofi Pasteur (ELM).

Conflict of interest

This manuscript describes the use of a platform provided on an early-access basis by Roche Sequencing Solutions. While scientists from Roche were involved in the experimental design and data analysis, the manuscript was prepared independently from Roche and did not require pre-approval from Roche prior to submission. RSP, EB, HL, JP, and JCT are employed by Roche Sequencing Solutions.

References

1. Chang HH, Huber RG, Bond PJ et al. Systematic analysis of protein identity between Zika virus and other arthropod-borne viruses. Bull World Health Organ. 2017;95:517-525I.
2. Xu X, Vaughan K, Weiskopf D et al. Identifying Candidate Targets of Immune Responses in Zika Virus Based on Homology to Epitopes in Other Flavivirus Species. PLoS Curr. 2016;8
3. Xu X, Song H, Qi J et al. Contribution of intertwined loop to membrane association revealed by Zika virus full-length NS1 structure. EMBO J. 2016;35:2170-2178.
4. Harrison SC. Immunogenic cross-talk between dengue and Zika viruses. Nat Immunol. 2016;17:1010-1012.

5. Safronetz D, Sloan A, Stein DR et al. Evaluation of 5 Commercially Available Zika Virus Immunoassays. Emerg Infect Dis. 2017;23:1577-1580.

6. Wong SJ, Furuya A, Zou J et al. A Multiplex Microsphere Immunoassay for Zika Virus Diagnosis. EBioMedicine. 2017;16:136-140.

7. Granger D, Hilgart H, Misner L et al. Serologic Testing for Zika Virus: Comparison of Three Zika Virus IgM-Screening Enzyme-Linked Immunosorbent Assays and Initial Laboratory Experiences. J Clin Microbiol. 2017;55:2127-2136.

8. Goncalves A, Peeling RW, Chu MC et al. Innovative and New Approaches to Laboratory Diagnosis of Zika and Dengue: A Meeting Report. J Infect Dis. 2018;217:1060-1068.

9. Lee AJ, Bhattacharya R, Scheuermann RH, Pickett BE. Identification of diagnostic peptide regions that distinguish Zika virus from related mosquito-borne Flaviviruses. PLoS One. 2017;12:e0178199.

10. Balmaseda A, Stettler K, Medialdea-Carrera R et al. Antibody-based assay discriminates Zika virus infection from other flaviviruses. Proc Natl Acad Sci U S A. 2017;114:8384-8389.

11. L'Huillier AG, Hamid-Allie A, Kristjanson E et al. Evaluation of Euroimmun Anti-Zika Virus IgM and IgG Enzyme-Linked Immunosorbent Assays for Zika Virus Serologic Testing. J Clin Microbiol. 2017;55:2462-2471.

12. Mishra N, Caciula A, Price A et al. Diagnosis of Zika Virus Infection by Peptide Array and Enzyme-Linked Immunosorbent Assay. MBio. 2018;9

13. Paixão ES, Teixeira MG, Rodrigues LC. Zika, chikungunya and dengue: the causes and threats of new and re-emerging arboviral diseases. BMJ Glob Health. 2018;3:e000530.

14. Carrillo-Hernández MY, Ruiz-Saenz J, Villamizar LJ, Gómez-Rangel SY, Martínez-Gutierrez M. Co-circulation and simultaneous co-infection of dengue, chikungunya,

and zika viruses in patients with febrile syndrome at the Colombian-Venezuelan border. BMC Infect Dis. 2018;18:61.

15. Azeredo EL, Dos Santos FB, Barbosa LS et al. Clinical and Laboratory Profile of Zika and Dengue Infected Patients: Lessons Learned From the Co-circulation of Dengue, Zika and Chikungunya in Brazil. PLoS Curr. 2018;10

16. Dudley DM, Aliota MT, Mohr EL et al. A rhesus macaque model of Asian-lineage Zika virus infection. Nat Commun. 2016;7:12204.

17. Nguyen SM, Antony KM, Dudley DM et al. Highly efficient maternal-fetal Zika virus transmission in pregnant rhesus macaques. PLoS Pathog. 2017;13:e1006378.

18. Martinot AJ, Abbink P, Afacan O et al. Fetal Neuropathology in Zika Virus-Infected Pregnant Female Rhesus Monkeys. Cell. 2018;173:1111-1122.e10.

19. Osuna CE, Lim SY, Deleage C et al. Zika viral dynamics and shedding in rhesus and cynomolgus macaques. Nat Med. 2016;22:1448-1455.

20. Hirsch AJ, Smith JL, Haese NN et al. Zika Virus infection of rhesus macaques leads to viral persistence in multiple tissues. PLoS Pathog. 2017;13:e1006219.

21. Hirsch AJ, Roberts VHJ, Grigsby PL et al. Zika virus infection in pregnant rhesus macaques causes placental dysfunction and immunopathology. Nat Commun. 2018;9:263.

22. Mohr EL, Block LN, Newman CM et al. Ocular and uteroplacental pathology in a macaque pregnancy with congenital Zika virus infection. PLoS One. 2018;13:e0190617.

23. Newman CM, Dudley DM, Aliota MT et al. Oropharyngeal mucosal transmission of Zika virus in rhesus macaques. Nat Commun. 2017;8:169.

24. Dudley DM, Newman CM, Lalli J et al. Infection via mosquito bite alters Zika virus tissue tropism and replication kinetics in rhesus macaques. Nat Commun. 2017;8:2096.

25. Haddow AD, Nalca A, Rossi FD et al. High Infection Rates for Adult Macaques after Intravaginal or Intrarectal Inoculation with Zika Virus. Emerg Infect Dis. 2017;23:1274-1281.

26. Adams Waldorf KM, Stencel-Baerenwald JE, Kapur RP et al. Fetal brain lesions after subcutaneous inoculation of Zika virus in a pregnant nonhuman primate. Nat Med. 2016;22:1256-1259.

27. Adams Waldorf KM, Nelson BR, Stencel-Baerenwald JE et al. Congenital Zika virus infection as a silent pathology with loss of neurogenic output in the fetal brain. Nat Med. 2018;24:368-374.

28. Coffey LL, Keesler RI, Pesavento PA et al. Intraamniotic Zika virus inoculation of pregnant rhesus macaques produces fetal neurologic disease. Nat Commun. 2018;9:2414.

29. Dudley DM, Van Rompay KK, Coffey LL et al. Miscarriage and stillbirth following maternal Zika virus infection in nonhuman primates. Nat Med. 2018;24:1104-1107.

30. Forsström B, Axnäs BB, Stengele KP et al. Proteome-wide epitope mapping of antibodies using ultra-dense peptide arrays. Mol Cell Proteomics. 2014;13:1585-1597.

31. Zandian A, Forsström B, Häggmark-Månberg A et al. Whole-Proteome Peptide Microarrays for Profiling Autoantibody Repertoires within Multiple Sclerosis and Narcolepsy. J Proteome Res. 2017;16:1300-1314.

32. Engmark M, Andersen MR, Laustsen AH et al. High-throughput immuno-profiling of mamba (Dendroaspis) venom toxin epitopes using high-density peptide microarrays. Sci Rep. 2016;6:36629.

33. Steffen W, Ko FC, Patel J et al. Discovery of a microbial transglutaminase enabling highly site-specific labeling of proteins. J Biol Chem. 2017;292:15622-15635.

34. Lyamichev VI, Goodrich LE, Sullivan EH et al. Stepwise Evolution Improves Identification of Diverse Peptides Binding to a Protein Target. Sci Rep. 2017;7:12116.

622 35. Christiansen A, Kringelum JV, Hansen CS et al. High-throughput sequencing
623 enhanced phage display enables the identification of patient-specific epitope motifs in
624 serum. Sci Rep. 2015;5:12913.
625 36. Tokarz R, Mishra N, Tagliafierro T et al. A multiplex serologic platform for diagnosis of
626 tick-borne diseases. Sci Rep. 2018;8:3158.
627 37. Bailey AL, Buechler CR, Matson DR et al. Pegivirus avoids immune recognition but
628 does not attenuate acute-phase disease in a macaque model of HIV infection. PLoS
629 Pathog. 2017;13:e1006692.
630 38. Aliota MT, Dudley DM, Newman CM et al. Heterologous Protection against Asian Zika
631 Virus Challenge in Rhesus Macaques. PLoS Negl Trop Dis. 2016;10:e0005168.
632 39. Aliota MT, Dudley DM, Newman CM et al. Molecularly barcoded Zika virus libraries to
633 probe in vivo evolutionary dynamics. PLoS Pathog. 2018;14:e1006964.
634 40. Braack L, Gouveia de Almeida AP, Cornel AJ, Swanepoel R, de Jager C. Mosquito-
635 borne arboviruses of African origin: review of key viruses and vectors. Parasit Vectors.
636 2018;11:29.
637 41. Pahar B, Kenway-Lynch CS, Marx P et al. Breadth and magnitude of antigen-specific
638 antibody responses in the control of plasma viremia in simian immunodeficiency virus
639 infected macaques. Virol J. 2016;13:200.
640 42. National Institutes of Allergy and Infectious Diseases. Immune Epitope Database and
641 Analysis Resource; 2018 [cited August 9, 2018]. Database: Immune Epitope
642 Database. Available from: www.iedb.org
643 43. De Winter, J.C.F. Using the Student's t-test with extremely small sample sizes.
644 Practical Assessment, Research & Evaluation 2013; 18:10
645 44. Lindsey NP, Staples JE, Powell K et al. Ability To Serologically Confirm Recent Zika
646 Virus Infection in Areas with Varying Past Incidence of Dengue Virus Infection in the
647 United States and U.S. Territories in 2016. J Clin Microbiol. 2018;56

45. Tsai WY, Youn HH, Brites C et al. Distinguishing Secondary Dengue Virus Infection From Zika Virus Infection With Previous Dengue by a Combination of 3 Simple Serological Tests. Clin Infect Dis. 2017;65:1829-1836.

46. Rönnberg B, Gustafsson Å, Vapalahti O et al. Compensating for cross-reactions using avidity and computation in a suspension multiplex immunoassay for serotyping of Zika versus other flavivirus infections. Med Microbiol Immunol. 2017;206:383-401.

47. Subissi L, Daudens-Vaysse E, Cassadou S et al. Revising rates of asymptomatic Zika virus infection based on sentinel surveillance data from French Overseas Territories. Int J Infect Dis. 2017;65:116-118.

48. Palmeira P, Quinello C, Silveira-Lessa AL, Zago CA, Carneiro-Sampaio M. IgG placental transfer in healthy and pathological pregnancies. Clin Dev Immunol. 2012;2012:985646.

49. Dai L, Song J, Lu X et al. Structures of the Zika Virus Envelope Protein and Its Complex with a Flavivirus Broadly Protective Antibody. Cell Host Microbe. 2016;19:696-704.

50. Barba-Spaeth G, Dejnirattisai W, Rouvinski A et al. Structural basis of potent Zika-dengue virus antibody cross-neutralization. Nature. 2016;536:48-53.

51. Ertürk M, Jennings R, Oxley KM, Hastings MJ. Effect of influenza A on phagocytic cell function. Med Microbiol Immunol. 1989;178:199-209.

52. Wang Q, Yang H, Liu X et al. Molecular determinants of human neutralizing antibodies isolated from a patient infected with Zika virus. Sci Transl Med. 2016;8:369ra179.

53. Zhang S, Kostyuchenko VA, Ng TS et al. Neutralization mechanism of a highly potent antibody against Zika virus. Nat Commun. 2016;7:13679.

54. Hasan SS, Miller A, Sapparapu G et al. A human antibody against Zika virus crosslinks the E protein to prevent infection. Nat Commun. 2017;8:14722.

55. Robbiani DF, Bozzacco L, Keeffe JR et al. Recurrent Potent Human Neutralizing Antibodies to Zika Virus in Brazil and Mexico. Cell. 2017;169:597-609.e11.

Supplemental material

Supplemental figure S1. SIV env epitopes identified by a high-density peptide microarray overlap known epitopes in variable loop regions. Serum from two Mauritian cynomolgus macaques (animals A1 and A2) before and after infection with SIVmac239 was evaluated for reactivity to overlapping peptides representing the SIVmac239 env protein sequence on a linear peptide microarray. SIV env variable loop regions [41] are highlighted in grey.

Supplemental figure S2. Reactivity of B1, C1, D1, and D2 against the complete polyprotein of ZIKV-FP. The $NS2B_{1427\text{-}1451}$RD25 epitope is highlighted in grey.

Supplemental figure S3. Reactivity of B1, C1, D1, and D2 against ZIKV-MR766 (A) and ZIKV-PR (B). The $NS2B_{1427\text{-}1451}$RD25 epitope is highlighted in grey.

Supplemental figure S4. ROC curves for best-performing epitope and multidimensional scaling (MDS) plot for different time points. ROC curves (A) were generated using data from the 8 animals analyzed against ZIKV polyproteins tiled as 16 amino acid peptides overlapping by 15 amino acids since this was the most complete dataset. ROC curves were created using the 8 samples collected at 0 DPI as the control group and the same 8 samples collected at 21-28 DPI samples as the test group. We chose consecutive peptides within the NS2B region that maximized the differences of mean log-normalized intensities between the controls and test

697 samples. The decision threshold was determined by maximizing the AUC and the resulting
698 ROCs of 9 to 13 peptides were plotted. ROC curves overlapped. MDS plots (B) of distances
699 between the log-normalized gene expression profiles were created using Limma plot MDS R
700 library. Only the 10 peptides in the identified $NS2B_{1427\text{-}1451}$RD25 epitope were used. Based on
701 MDS analysis, pre-infection samples (blue), samples from early convalescence (21-28 dpi, red),
702 and samples from any later time (>43 dpi, yellow) clustered in separate groups.
703
704 **Supplemental figure S5.** Reactivity of cohort G (ZIKV-FP infection during first trimester), H
705 (ZIKV-PR infection during first trimester), and I (history of DENV-3 infection, ZIKV-PR infection
706 during first trimester) against the ZIKV-FP polyprotein. The $NS2B_{1427\text{-}1451}$RD25 epitope is
707 highlighted in grey.
708
709 **Supplemental figure S6.** Reactivity of cohort G (ZIKV-FP infection during first trimester), H
710 (ZIKV-PR infection during first trimester), and I (history of DENV-3 infection, ZIKV-PR infection
711 during first trimester) against the DENV-2 polyprotein. The region of the DENV-2 polyprotein
712 corresponding to the ZIKV $NS2B_{1427\text{-}1451}$RD25 epitope is highlighted in grey.
713
714 **Supplemental Table S7.** Arboviral proteins and polyproteins used for CDF plot analysis.

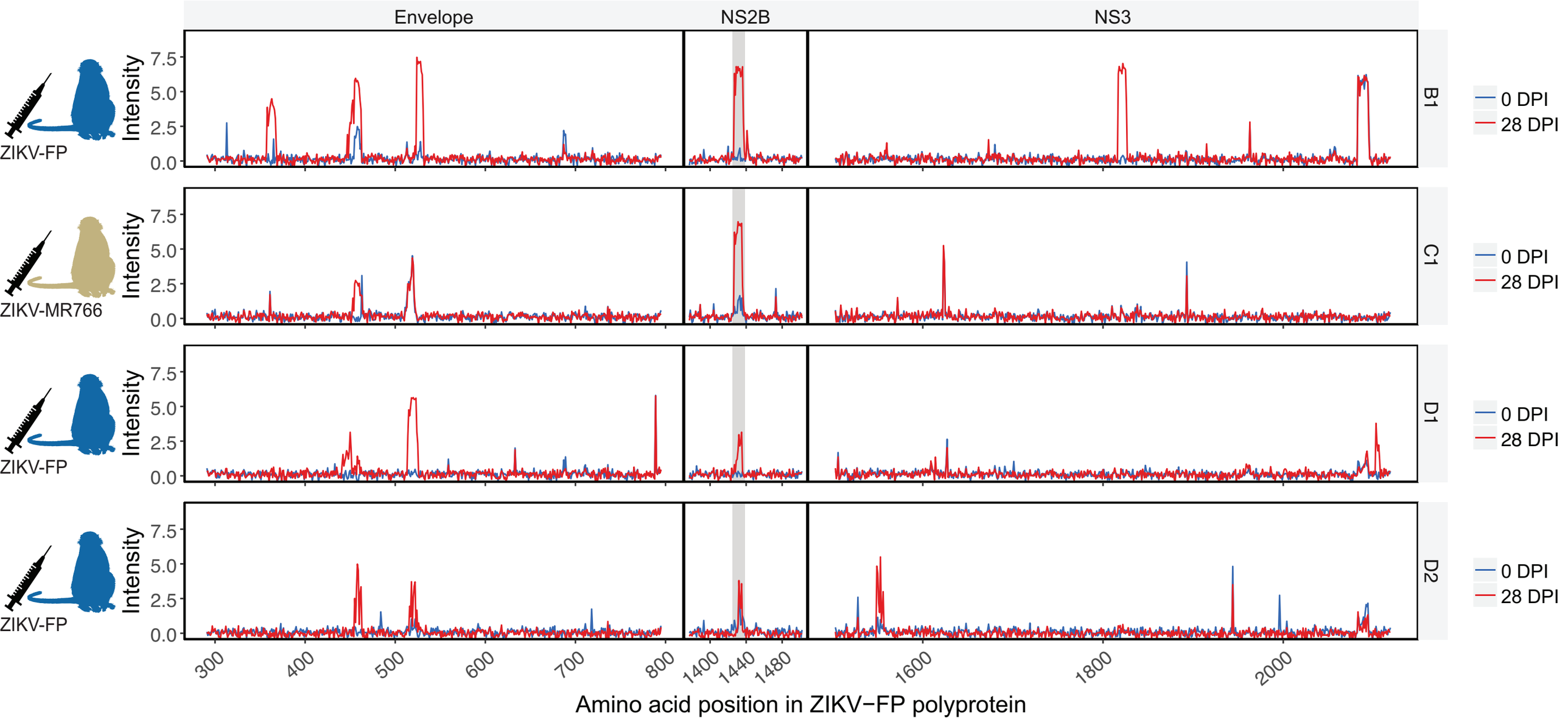
Envelope
NS2B
NS3
ZIKV-FP
ZIKV-MR766
ZIKV-FP
ZIKV-FP
Intensity
7.5
5.0
2.5
0.0
B1
C1
D1
D2
0 DPI
28 DPI
300
400
500
600
700
800
1400
1440
1480
1600
1800
2000
Amino acid position in ZIKV−FP polyprotein

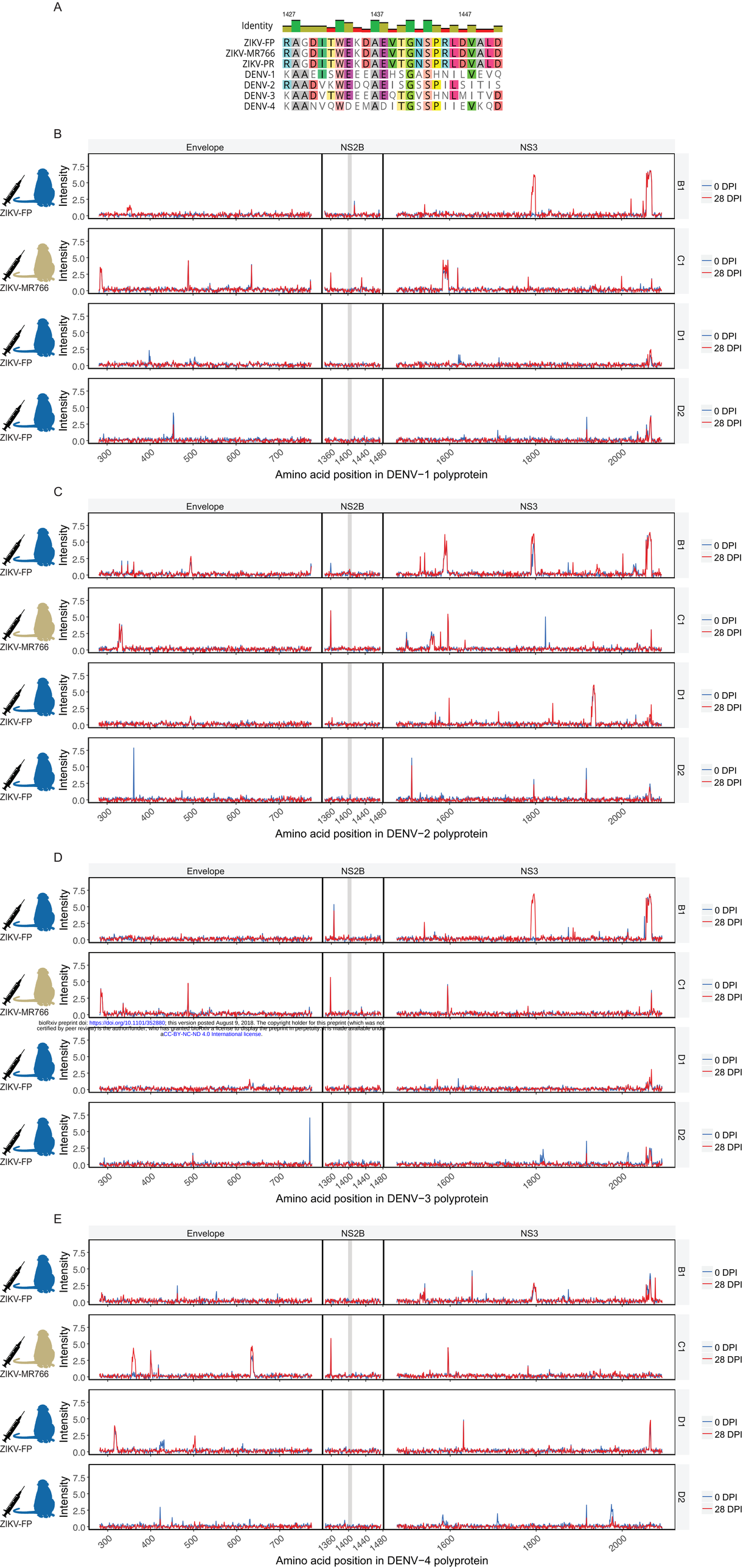

A

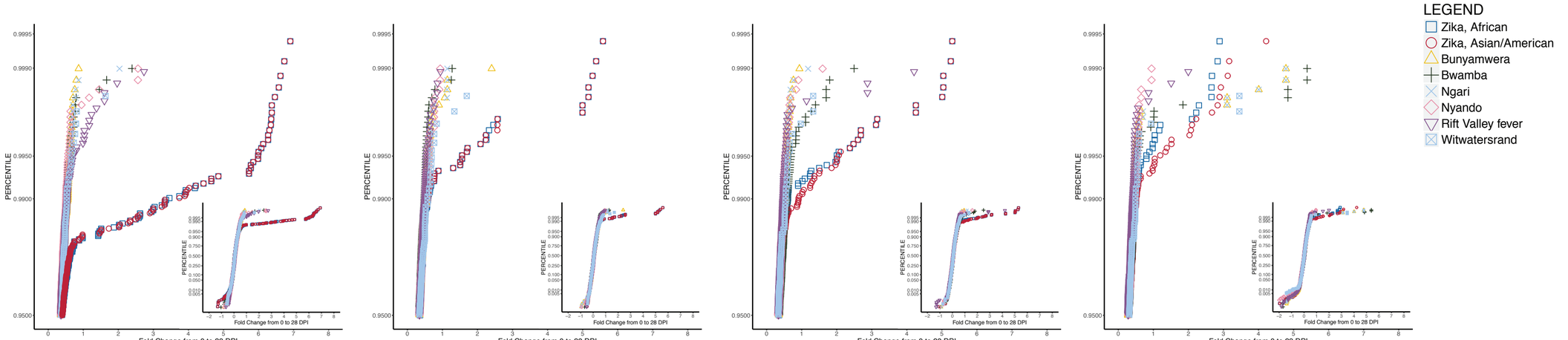

B

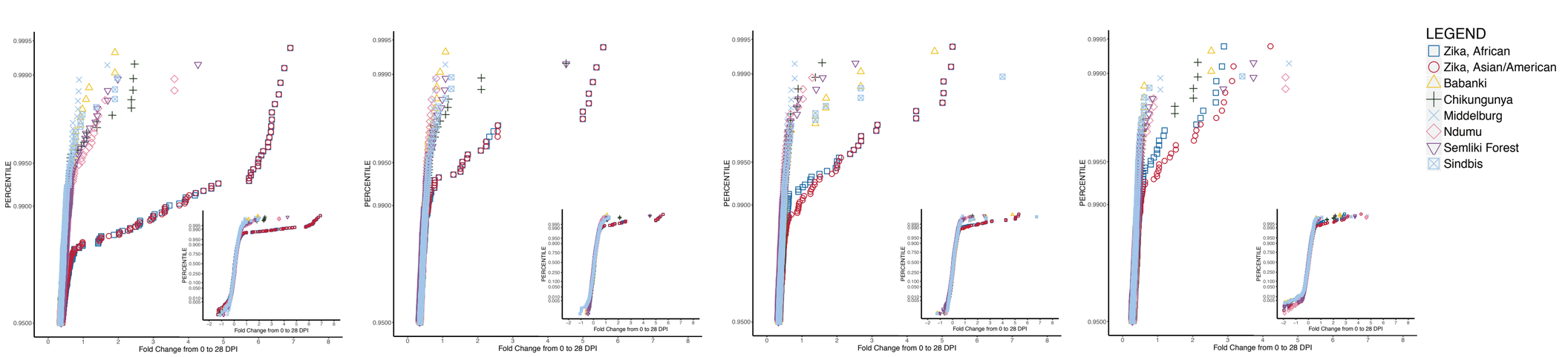

C

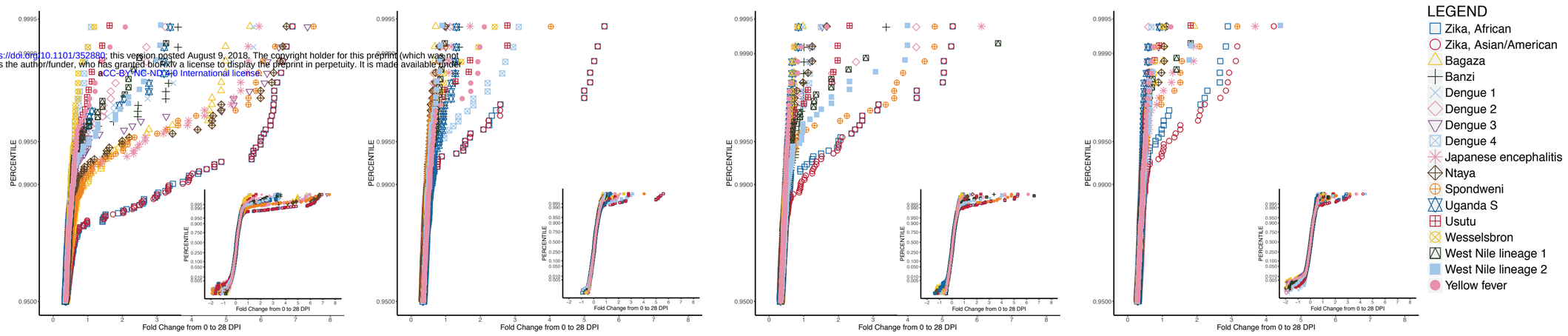

D

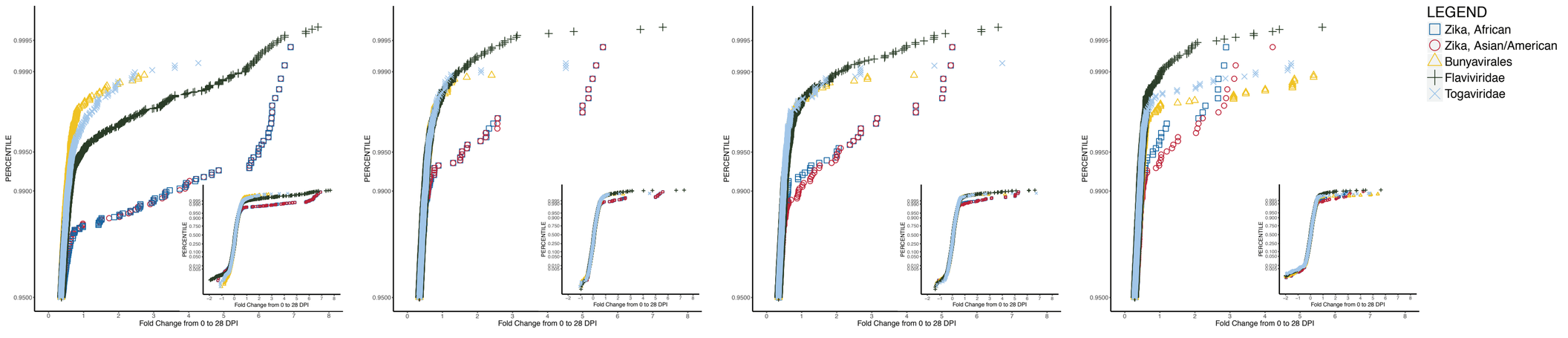

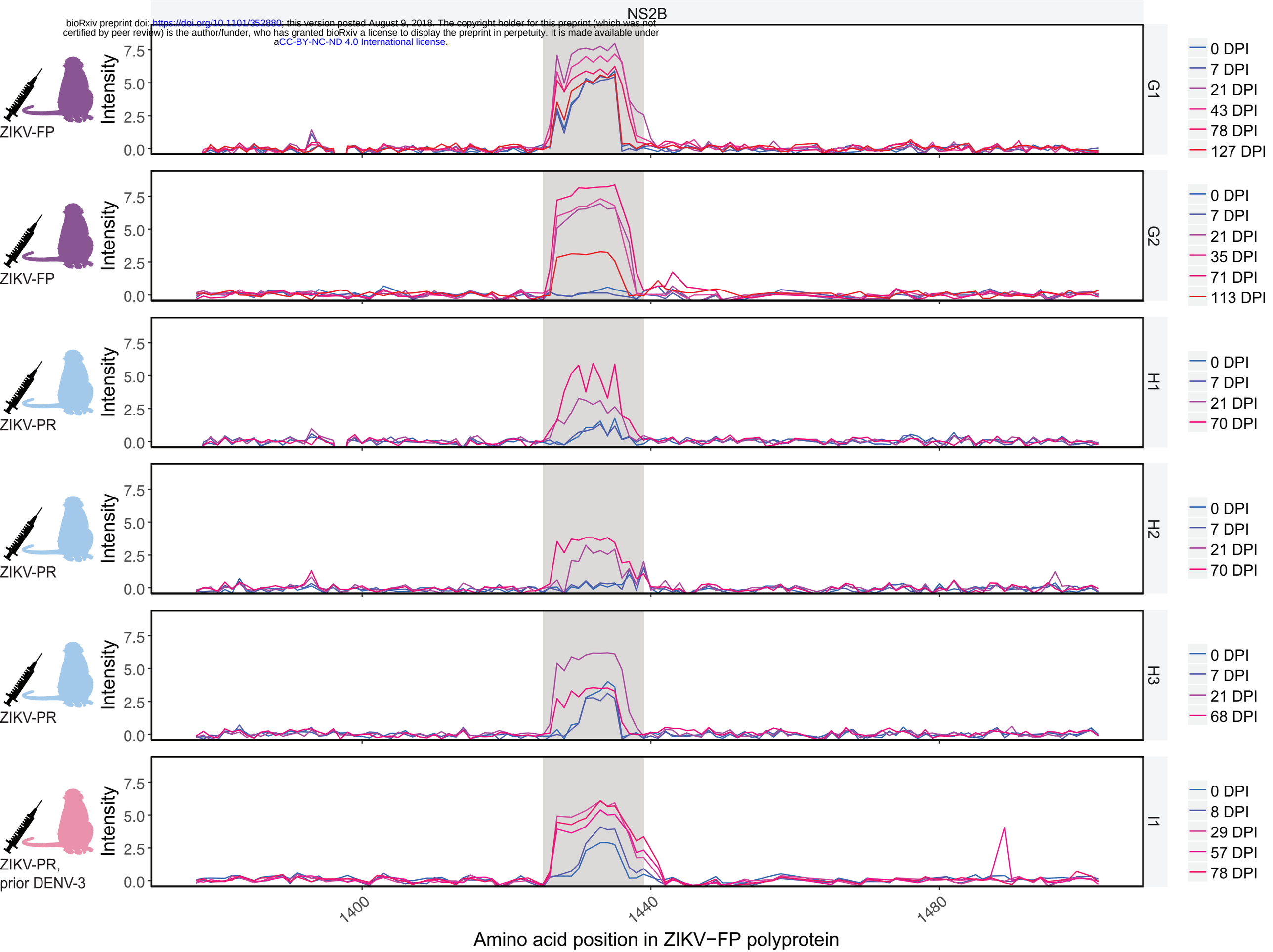

A

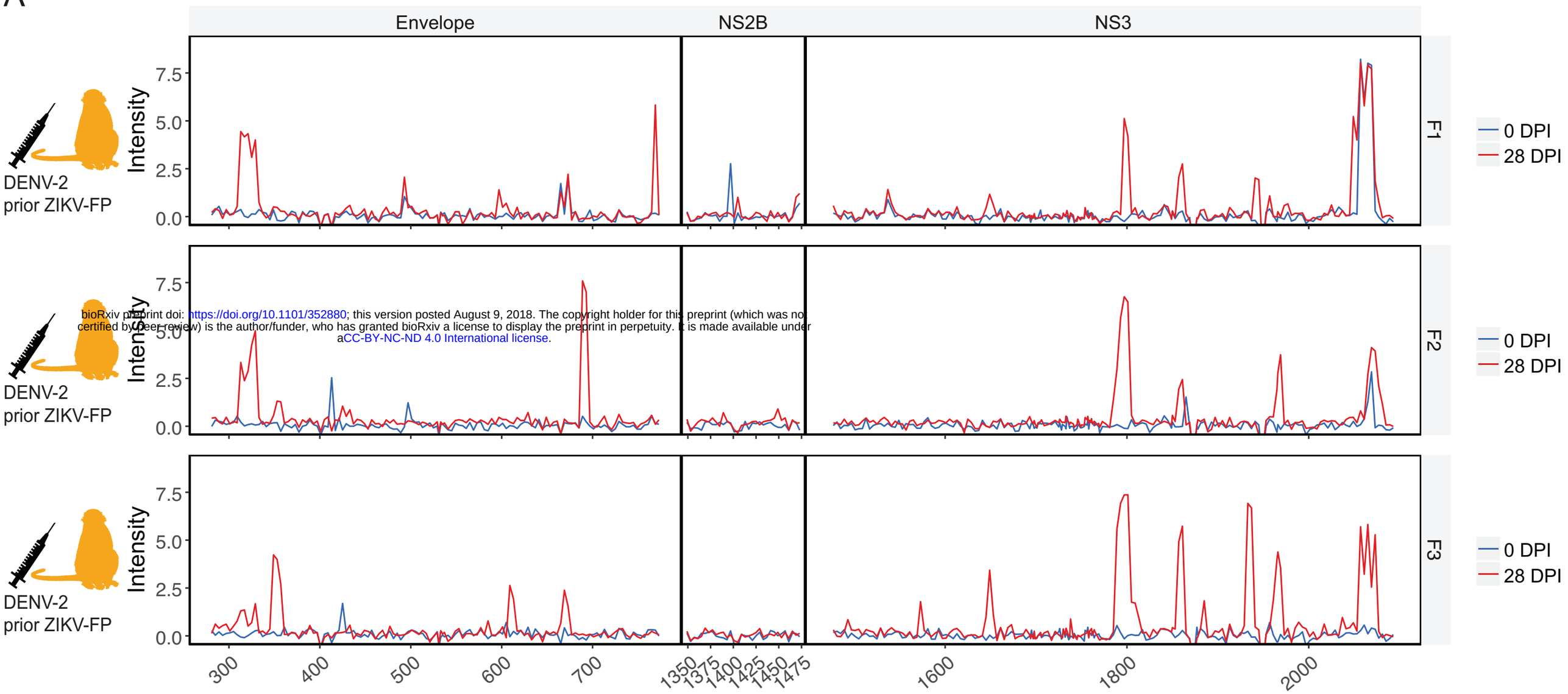

B